PHYSICS OF FLUIDS VOLUME 13, NUMBER 10 OCTOBER 2001

Numerical simulation of particle-laden turbulent channel flow

Yiming Li and J. B. McLaughlin
Department of Chemical Engineering, Clarkson University, Potsdam, New York 13699-5705

K. Kontomaris
DuPont Central Research and Development, Wilmington, Delaware 19880-0249

L. Portela
Kramers Laboratory, Delft University of Technology, Delft, The Netherlands

(Received 30 November 1999; accepted 29 June 2001)

This paper presents results for the behavior of particle-laden gases in a small Reynolds number vertical channel down flow. Results will be presented for the effects of particle feedback on the gas-phase turbulence and for the concentration profile of the particles. The effects of density ratio, mass loading, and particle inertia will be discussed. The results were obtained from a numerical simulation that included the effects of particle feedback on the gas phase and particle–particle collisions. The resolution of the simulation was comparable to the smallest scales in the particle-free flow, but the grid spacings were larger than the particle size. Particle mass loadings up to 2 and both elastic and inelastic collisions were considered. Particle feedback causes the turbulent intensities to become more anisotropic as the particle loading is increased. For small mass loadings, the particles cause an increase in the gas flow rate. It will be shown that the particles tend to increase the characteristic length scales of the fluctuations in the streamwise component of velocity and that this reduces the transfer of turbulent energy between the streamwise component of velocity and the components transverse to the flow. Particle–particle collisions greatly reduce the tendency of particles to accumulate at the wall for the range of mass loadings considered. This was true even when the collisions were inelastic.
[DOI: 10.1063/1.1396846]

I. INTRODUCTION

When small suspended particles are present at sufficient concentrations in a turbulent flow, they can modify the structure of the turbulence. In the case of turbulent gas flow, one can identify three regimes of particle mass loading, m_s, in which $m_s \ll 1$, $m_s = O(1)$, or $m_s \gg 1$. In this paper, the particle mass loading is defined to be the ratio of the mass of the particles to the mass of the gas in the computational domain. When $m_s \ll 1$, one can expect the effect of the particles on the gas phase to be small. When $m_s = O(1)$, the particles will affect the gas flow. However, the particle volume fraction, Φ_v, is very small compared to unity. Therefore, one can, to a first approximation, ignore the volume occupied by the particles in simulating the gas flow. Provided the particle size is sufficiently small, one can expect that the particles will tend to suppress gas-phase turbulence according to the criteria suggested by Hetsroni[1] and Gore and Crowe.[2]

Squires and Eaton[3] and Elghobashi and Truesdell[4] reported the results of particle feedback on homogeneous gas turbulence. In both cases, the particles were sufficiently small that, following Crowe *et al.*,[5] they could be modeled as point forces acting on the fluid (the Particle-Source in Cell "PSIC" method). Pan and Banerjee[6] used a higher order method to investigate particle feedback on liquids in a turbulent open channel flow. Maxey and Patel[7] developed methods for simulating suspensions of small particles in liquids in which the forces coupling the two phases were distributed over a finite volume. These methods were used by Maxey *et al.*[8] to perform simulations of particles and bubbles in homogeneous turbulence.

The results presented in this paper were obtained using the PSIC method to simulate particle feedback in a turbulent channel flow. The orientation of the channel was vertical and the flow of air was downward to facilitate comparison with Kulick *et al.*[9] The particles were either glass or copper with sizes ranging from 12 to 39 μm. The particle mass loading was varied over the range 0–2. The effects of particle–wall and particle–particle collisions were considered. In most cases, the collisions were assumed to be elastic. The techniques used to include particle–particle collisions are similar to the techniques described by Chen *et al.*[10,11] for droplet–droplet collisions.

Kulick *et al.*[9] reported the results of experiments on particle-laden flows in a vertical channel flow. Unlike the simulations in this work, for which the pressure gradient was fixed, the bulk flow rate was fixed in their experiments. The corresponding Reynolds number was approximately 50 000, while the Reynolds number in the work to be presented was roughly 7000. Here, the Reynolds number, Re_b is based on the hydraulic diameter of the channel (twice the channel width) and the bulk velocity. The friction velocity was 49 cm/s in both the experiments and the simulations. Kulick *et al.* performed experiments on both glass and copper particles in downward air flows. The particles used in their experiments were larger than the particles used in the simula-

1070-6631/2001/13(10)/2957/11/$18.00

tions. Therefore, only qualitative comparisons can be made between the computed results and the experimental results.

Yamamoto *et al.*[12] reported LES results for a channel flow at approximately the same Reynolds number as in Kulick *et al.* experiments. They considered 50 micron glass particles, 70 micron copper particles, and 28 micron lycopodium particles in their simulations. They also included elastic particle–particle collisions in their simulations. They considered particle mass loadings equal to 0.01, 0.2, and 0.4. Their study focused in the tendency of particles to cluster. They found that particles with the least inertia showed the greatest tendency to form clusters. They found that particle–particle collisions and two-way coupling reduced the tendency of particles to concentrate in low speed streaks in the viscous sublayer. In the channel center, the size and shape of particle clusters predicted by the simulations were in reasonable agreement with the experiments.

The present study differs in several respects from that of Yamamoto *et al.* First, the Reynolds number is much smaller and no subgrid scale modeling was used in the simulations. A second difference is that the particles have less inertia, as measured by the Stokes relaxation time, than the particles considered by Yamamoto *et al.* The present paper presents concentration profiles for the particles after steady-state conditions are reached, while Yamamoto *et al.* show the instantaneous locations of the particles in various planes. Finally, much of the present paper focuses on the effects of the particles on the gas-phase turbulence.

Sommerfeld[13] described a stochastic method for computing particle trajectories which incorporated particle–particle collisions. His results indicated that particle–particle collisions play an important role in redispersing particles that tend to accumulate near the lower wall of a horizontal channel flow.

II. METHODOLOGY

A. Gas phase

The gas phase is assumed to satisfy a modified Navier–Stokes equation in which the feedback force on the gas is included as an effective body force

$$\frac{\partial \mathbf{u}}{\partial t}+\mathbf{u}\cdot\nabla\mathbf{u}=-\nabla p/\rho_g-\frac{dP}{dx}\hat{x}+v\nabla^2\mathbf{u}+\mathbf{f}^r. \tag{1}$$

In Eq. (1), the symbols $\mathbf{u}$, t, p, P, ρ_g, v, and $\mathbf{f}^r$ denote the gas velocity, time, fluctuating pressure, external pressure, gas density, viscosity, and the feedback force per unit mass, respectively.

To compute the feedback force per unit mass, the computational domain is divided into imaginary rectangular regions. Each of these imaginary regions contains one grid point. The reaction forces exerted by the particles in each region are summed and the sum is divided by the mass of gas contained in the volume. The reaction force of a particle was the negative of the sum of the drag and lift forces acting on the particle.

The gas phase is assumed to be incompressible

$$\nabla\cdot\mathbf{u}=0. \tag{2}$$

The gas velocity field satisfies no-slip boundary conditions on the channel walls and periodic boundary conditions in the downstream (x) and spanwise (z) directions.

B. Particles

The particle equation of motion was described in detail by Chen and McLaughlin.[14] The effects of drag, lift, and gravity are included in the equation. The drag law incorporates a nonlinear correction to account for finite particle Reynolds numbers. The drag force included wall corrections that are important when a particle is a few diameters particle diameters from the closest wall. The lift force also incorporated wall corrections. Particle–particle collisions are not directly described in the particle equation of motion; they will be discussed in the following section.

The particle relaxation time, τ, is a useful way of characterizing particle inertia. In the Stokes flow limit, the drag force on a particle may be expressed as

$$\mathbf{F_d}=-\frac{1}{\tau}(\mathbf{v}-\mathbf{u}), \tag{3}$$

where

$$\tau=\frac{2\rho_p/\rho_g+1}{9}\frac{a^2}{v}. \tag{4}$$

In Eqs. (3) and (4), $\mathbf{v}$ is the particle velocity, a is the particle radius, ρ_g is the gas density, ρ_p is the particle density, and v is the kinematic viscosity. In the Stokes flow regime, if a particle is projected into a quiescent fluid with a horizontal velocity v_0, it will travel a horizontal distance equal to $v_0\tau$.

In all but two of the simulations to be described, particle–particle and particle–wall collisions were assumed to be elastic. To assess the importance of inelastic collisions on the results, two simulations were performed in which the normal component of the post-collision velocity was multiplied by a coefficient of restitution, e. The same value of e was used for particle–particle and particle–wall collisions.

III. NUMERICAL METHODS

The gas-phase equations were solved using pseudospectral methods. With the exception of the feedback force, the techniques are essentially the same as those described by McLaughlin[15] and Lyons *et al.*[16] The velocity and pressure fields were expanded in Fourier series in the x and z directions and Chebyshev series in the y direction. The equations were discretized in time using a fractional step method in which (1) the nonlinear, external pressure gradient, and feedback terms were evaluated; (2) the fluctuating pressure term was evaluated; (3) the viscous term was evaluated.

The trajectory of each particle was computed simultaneously in time with the gas-phase equations. This was done by solving the equations for the particle velocity and position vectors for each particle

$$m\frac{d\mathbf{v}}{dt}=\mathbf{F_d}+\mathbf{F_1}+\mathbf{F_g}, \tag{5}$$

$$\frac{d\mathbf{r}}{dt} = \mathbf{v}. \tag{6}$$

In Eqs. (5) and (6), m denotes the particle mass, $\mathbf{v}$ is the particle velocity, $\mathbf{F_d}$ is the drag force, $\mathbf{F_l}$ is the lift force, $\mathbf{F_g}$ is the gravitational force, and $\mathbf{r}$ is the position vector. The above equations were discretized in time and solved to compute tentative values for the particle velocity and position vectors on each time step. Using the tentative values and the assumption that each particle moved along a straight line for one time step, the possibility of particle–particle or particle–wall collisions was considered. The procedure for this was essentially the same as that described by Chen *et al.*[10] The only modification was that the channel was divided into a three-dimensional lattice of cells and the head of chain-linked lists algorithm described by Hockney and Eastwood[17] was used to search for possible collisions between each particle and the particles in the same cell or the neighboring cells. When a particle–particle collision was identified, the final coordinates and velocities of the colliding particles were modified to account for the collision. In all but two simulations, the collisions were taken to be elastic. The volume fractions were sufficiently small $(O(10^{-3}))$ that, over a time step, multiple collisions were extremely rare. In a typical run, the collision calculations used about 5% of the total CPU time.

IV. PARAMETER CHOICES

It is useful to introduce nondimensional variables based on "wall units." Such dimensionless variables will be denoted by a + superscript. The units of length and time are υ/u_* and υ/u_*^2, where υ and u_* denote the kinematic viscosity and the friction velocity of the particle-free gas flow. The external pressure gradient was the same for all the simulations. For the particle-free gas, the pressure gradient balances the wall shear stress and the friction velocity used to nondimensionalize the variables in all simulations was the friction velocity for the particle-free case. When particles are present, the wall shear stress must balance the weight of the particles as well as the external pressure gradient. Thus, the friction velocity based on the wall shear stress in these cases is larger than for the particle-free case. This point will be discussed quantitatively in Sec. VI.

In these units, the channel half-width is $h^+ = 125$ and the downstream and spanwise periods are $X^+ = 1260$ and $Z^+ = 630$. The numbers of grid points in the x, y, and z directions were 32, 65, and 64, respectively. For all simulations, the fluid was air at ambient conditions and the friction velocity of the particle-free case was 49 cm/s. For this friction velocity, $l_* = 3.06\times10^{-3}$ cm and $t_* = 6.25\times10^{-5}$ s. The input parameters for the fluid and flow conditions are summarized in Table I.

TABLE I. Input parameters for the fluid (ambient air) and the flow conditions.

P (atm)	T (K)	υ (cm^2/s)	ρ_g (g/cm^3)	u_* (cm/s)	h (cm)	X (cm)	Z (cm)
1	298	0.15	1.2×10^{-3}	49	0.383	3.86	1.93

TABLE II. Run matrix.

Run ID	Solid	e	d (μm)	d^+	τ^+	m_s	N
1	none	⋯	⋯	⋯	⋯	⋯	⋯
2	glass	1	22	0.714	59	0.20	100 000
3	glass	1	39	1.29	192	0.20	17 000
4	glass	1	39	1.29	192	0.40	34 000
5	copper	1	21	0.686	192	0.20	32 000
6	glass	no collision	39	1.29	192	0.20	17 000
7	glass	0.9	39	1.29	192	0.40	34 000
8	glass	0.9	39	1.29	192	2.0	170 000
9	glass	1.0	39	1.29	192	2.0	170 000

Results are reported for glass and copper particles. The densities of glass and copper were taken to be 2.5 and 8.8 g/cm^3. The values of ρ_p/ρ_g for glass and copper were 2083 and 7333, respectively. The run matrix in Table II summarizes the simulation parameters. In Table II, the parameter N is the number of particles traced in the simulations.

Each simulation was performed for 10 000 time steps. The dimensionless time step was 0.25. Thus, the period of a simulation was 2500. The interval from 1500 to 2500 was used to compute statistics since it was desired to obtain steady-state results.

V. RESULTS

In Fig. 1, the mean gas velocity, U^+, is plotted against the distance from the closest channel wall, y^+, for $m_s = 0$, 0.2, and 0.4. The plots are for 39 μm glass particles $(\tau^+ = 192)$. Since the external pressure gradient is fixed, it may be seen that the addition of particles produces an increase in the mean gas velocity.

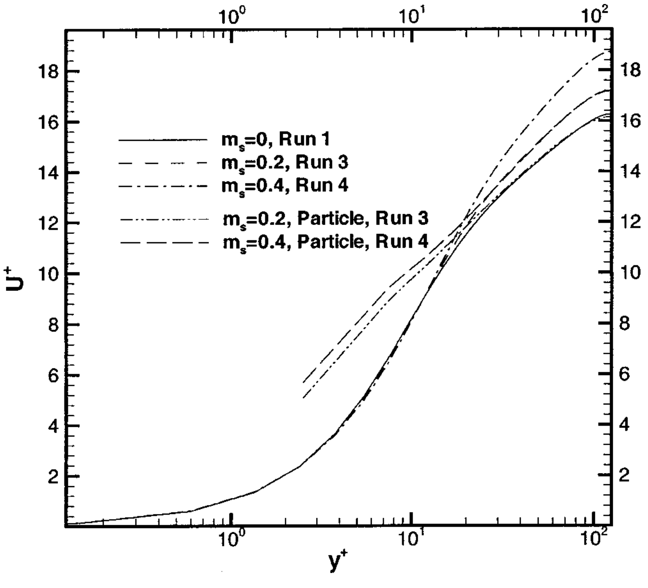

FIG. 1. Effect of solids mass loading on the mean gas velocity and the mean particle velocity for small mass loadings, glass, $\tau^+ = 192$.

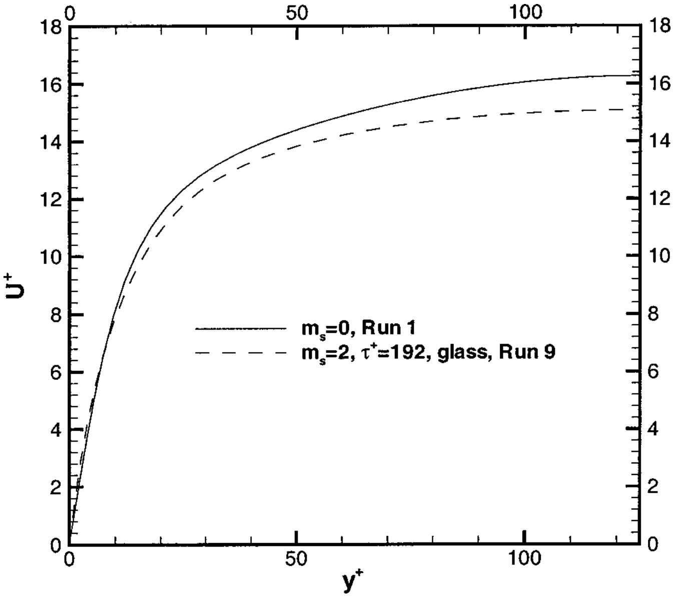

FIG. 2. Effect of solids mass loading on the mean gas velocity for $m_s = 2$, glass, $\tau^+ = 192$.

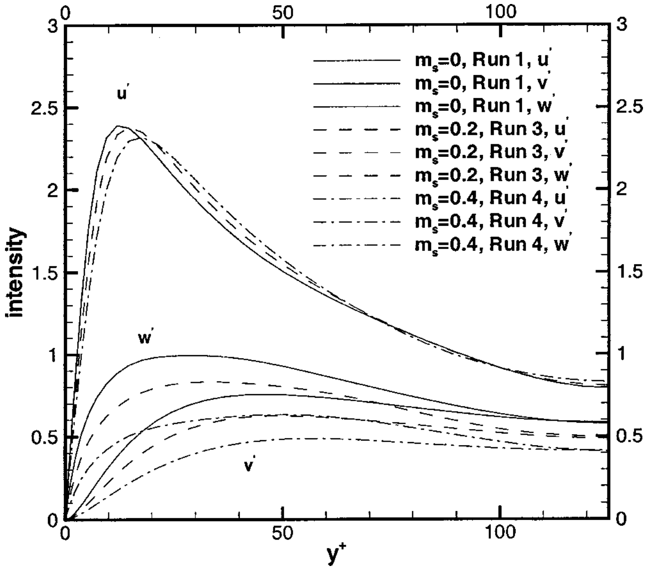

FIG. 3. Effect of solids mass loading on the fluid turbulent intensities (in wall units) for small mass loadings, glass, $\tau^+ = 192$.

The mean particle velocity is also plotted in Fig. 1. It may be seen that the particles lag the fluid in the core of the channel, but they lead the fluid in the near wall region. This phenomenon has been reported by Kulick *et al.*[9] The slip velocity can be quite large in the viscous wall region and leads to relatively large Reynolds numbers. For both the glass particles in Fig. 1 and the copper particles to be discussed later, the average particle Reynolds number in the viscous sublayer was about 5. For the smaller glass particles, the corresponding Reynolds number was about 2.

Figure 2 shows the mean velocity profile for the same glass particles as in Fig. 1, but at $m_s = 2$. It may be seen that, unlike the behavior observed for smaller mass loadings, the particles reduce the mean gas velocity.

Figure 3 shows the fluid turbulence intensities versus y^+ for the same cases shown in Fig. 1. It is seen that the effect on the fluctuation intensities is anisotropic; the disparity between the normal and spanwise fluctuations and the streamwise fluctuations is increased. The maxima of the three intensities move further from the wall and become broader as the particle mass loading increases. This behavior is also consistent with the experimental observations of Kulick *et al.*[9]

Figure 4 shows the fluid turbulence intensities versus y^+ for the same glass particles as in Fig. 3, but with $m_s = 2$. In contrast to the smaller mass loadings shown in Fig. 3, the particles strongly suppress the gas-phase turbulence fluctuations in all three components of velocity. Also, unlike the behavior for small mass loadings, the maxima have moved closer to the wall.

Figure 5 shows the fluid turbulence intensities as a function of y^+ for glass particles with two different values of τ^+. The results for the particle-free case are shown for comparison. It may be seen that the particles with more inertia have a smaller effect on the turbulent fluctuations. The smaller particles significantly enhance the intensity of the fluctuations in the streamwise component of the velocity.

Figure 6 shows the fluid turbulence intensities as a function of y^+ for copper and glass particles. For both cases, $\tau^+ = 192$. Thus, the difference between the two simulations shows the effect of the density ratio, ρ_p/ρ_g, or, equivalently, the particle diameter, d^+. The copper particles have a smaller effect on the normal and spanwise components of velocity than the glass particles. Both types of particles have a relatively small effect on the intensity of the streamwise component of velocity.

The presence of particles has a significant effect on the streamwise correlation of the streamwise component of velocity. This may be seen in Fig. 7 which shows the quantity $R_{uu}(x^+)$ which is defined by

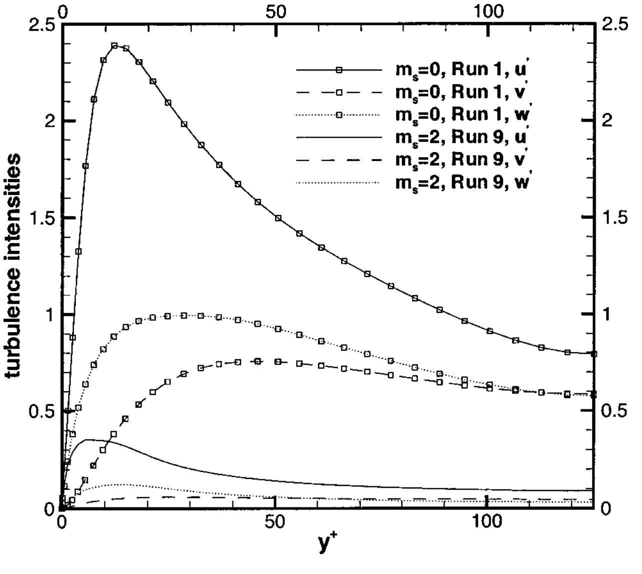

FIG. 4. Effect of solids mass loading on the fluid turbulent intensities (in wall units) for $m_s = 2$, glass, $\tau^+ = 192$.

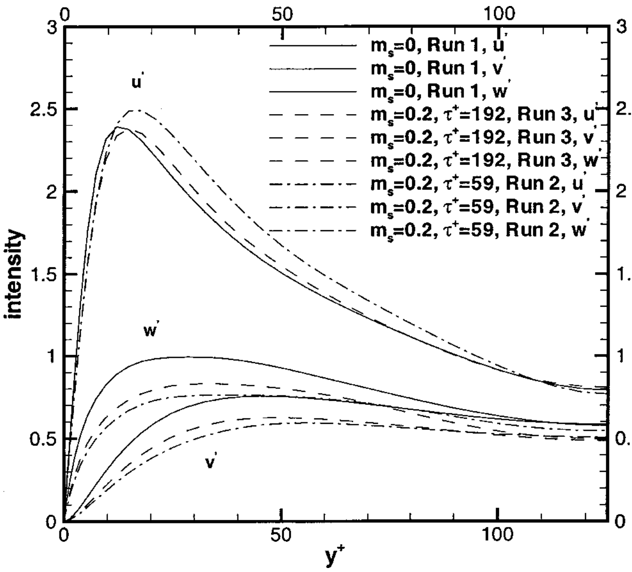

FIG. 5. Effect of particle inertia on the fluid turbulent intensities (in wall units), $m_s=0.2$, $\tau^+=192$.

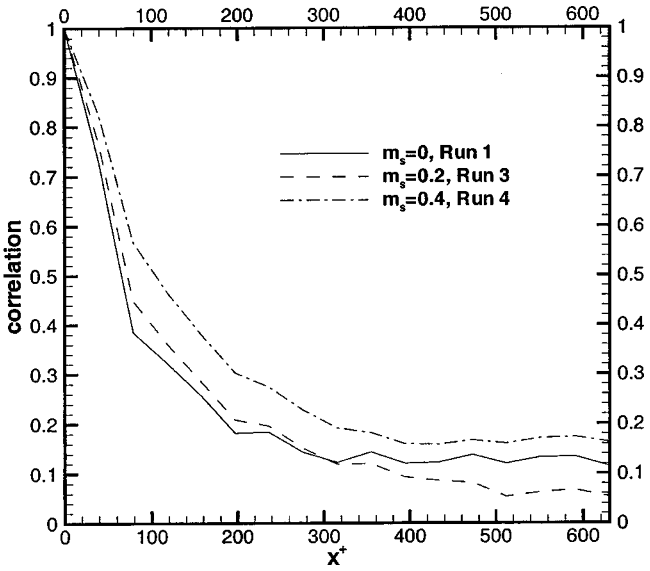

FIG. 7. Streamwise correlation coefficient, $R_{uu}(x^+)$, for $y^+=41$, $\tau^+=192$, glass.

$$R_{uu}(x^+)=\langle u^+(x'^+,y^+,z^+,t^+)\times u^+(x'^++x^+,y^+,z^+,t)\rangle/(u'^+)^2, \tag{7}$$

where u is the fluctuating part of the x component of the gas velocity, as a function of the streamwise separations, x^+ and the angle brackets denote averaging over time and x'^+ and z^+. The curves are plotted for $y^+=41$. Results are shown for $m_s=0$, 0.2, and 0.4. The differences between the computed correlations for $m_s=0$ and 0.2 are comparable to the statistical uncertainty in the correlations. However, for $m_s=0.4$, the correlation is consistently larger than for $m_s=0$.

By contrast, the particles have relatively little effect on the spanwise correlation of the streamwise component of velocity as may be seen in Fig. 8, which shows the correlation function at $y^+=3.75$. For all mass loadings, it may be seen that the correlation has a minimum for a spanwise spacing that is close to 50 wall units. This is consistent with a streak spacing equal to 100 wall units in the viscous sublayer.

Figures 9 and 10 indicate that the particles have a smoothing effect on fluctuations in the streamwise direction. Figures 9 and 10 show instantaneous views of the contours of the fluctuating part of the x component of velocity in a plane for which $y^+=41$. Figure 9 shows the contours for a particle-free flow, while Fig. 10 shows the contours for $m_s=0.4$. For $m_s=0.4$, the contours are consistent with the suppression of small scales in the x direction.

Finally, Table III gives the computed values of the centerline velocity, the bulk velocity, and the Reynolds number. These values were obtained from the dimensionless velocity profile.

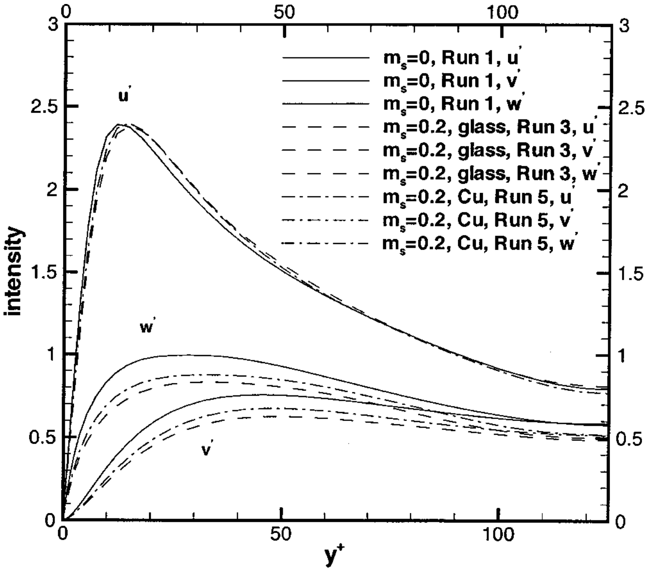

FIG. 6. Effect of density ratio (or diameter) on the fluid turbulent intensities (in wall units), $m_s=0.2$, $\tau^+=192$.

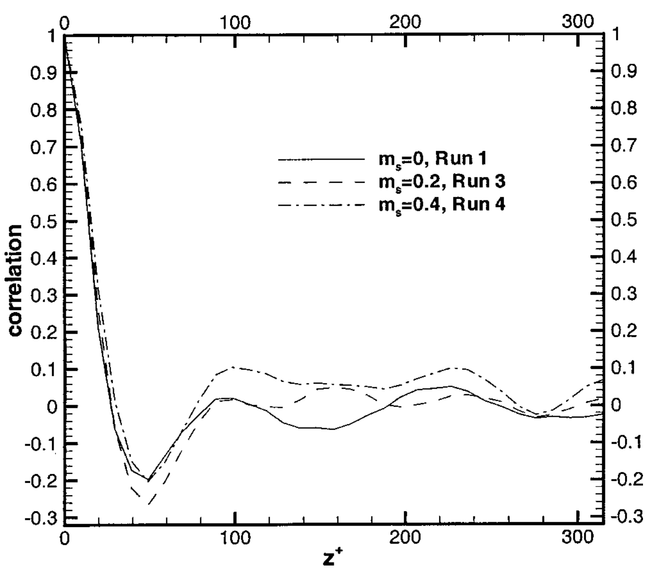

FIG. 8. Spanwise correlation coefficient, $R_{uu}(z^+)$, for $y^+=3.75$, $\tau^+=192$, glass.

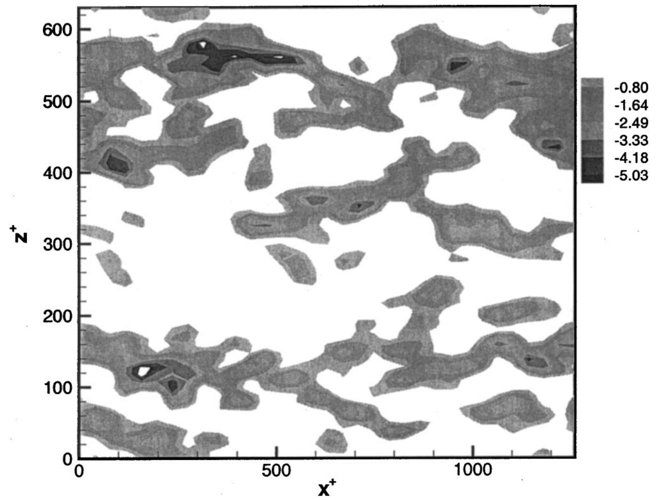

FIG. 9. Instantaneous contours of u^+ in a plane for which $y^+=41$, particle-free.

Particles in the size range considered have a tendency to accumulate near the channel walls even though they were homogeneously distributed at the beginning of each run. This is apparent in Fig. 11 which shows the normalized particle concentration as a function of y^+. The plots in Fig. 11 were obtained from the final coordinates of the particles in Runs 3 and 4. The concentration was normalized by the initial concentration of particles, which was uniform. In each case, the particle concentration near the wall is significantly larger than the particle concentration in the core. The concentration near the wall is smaller for $m_s=0.4$ than for $m_s=0.2$.

VI. DISCUSSION

A. Particle feedback effects on the gas phase

TABLE III. Computed results for the gas flow.

Run ID	U_c (m/s)	U_b (m/s)	Re_b	τ_w^+	$\tau_{w,\mathrm{th}}^+$
1	7.99	6.71	6869	1.007	1.0
2	8.53	7.20	7328	1.012	1.031
3	8.43	7.06	7213	1.029	1.031
4	9.16	7.60	7732	1.073	1.062
5	8.38	7.06	7187	1.043	1.031
6	8.33	7.01	7137	1.035	1.031
7	8.97	7.55	7681	1.044	1.031
8	7.49	6.61	6760	1.33	1.31
9	7.40	6.61	6754	1.31	1.31

The particles produce an increase in the mean gas velocity and the corresponding bulk flow rate. Table III gives the bulk velocity and Reynolds number. The external pressure gradient had the same value in all runs. However, when particles are present, the wall shear stress must balance both the external pressure gradient and the weight of the particles. In terms of dimensional variables, this balance takes the following form:

$$-\frac{dP}{dx}=\frac{\tau_w}{h}-m_s\rho_g g, \tag{8}$$

where g is the acceleration of gravity and τ_w is the wall shear stress. If one makes the variables dimensionless in terms of the friction velocity of the particle-free flow, u_*, one can express the balance as follows:

$$\left.\frac{dU^+}{dy^+}\right|_w=1+\frac{m_s}{2\mathrm{Fr}}, \tag{9}$$

where the Froude number, Fr, is defined by

$$\mathrm{Fr}=\frac{u_*^2}{2hg}, \tag{10}$$

where the subscript "w" indicates that the quantity is evaluated at a wall. The nondimensional velocity gradient at the wall is equal to the nondimensional wall shear stress, τ_w^+. Equation (9) states, in dimensionless form, that the shear stress at the wall balances both the external pressure gradient

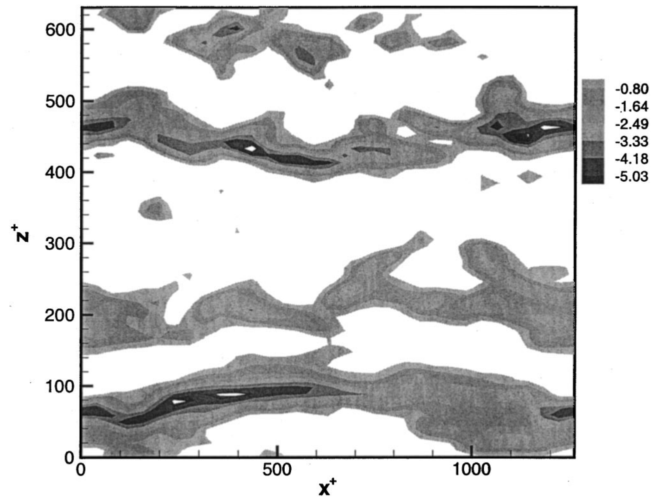

FIG. 10. Instantaneous contours of u^+ in a plane for which $y^+=41$, $\tau^+=192$, $m_s=0.4$, glass.

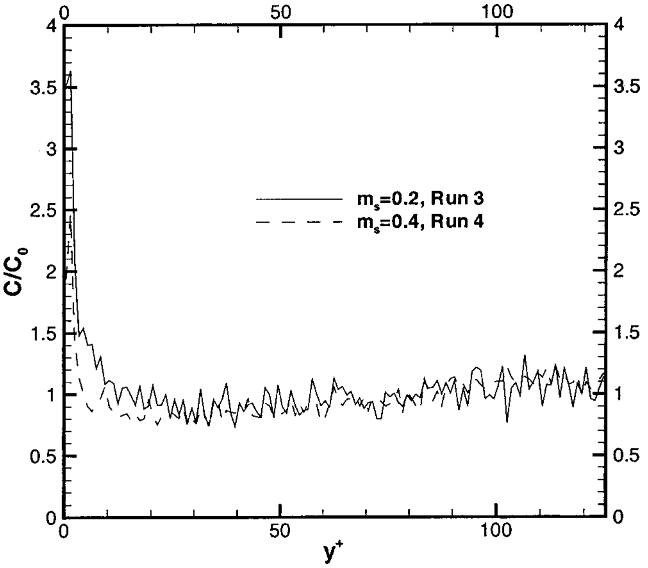

FIG. 11. Normalized particle concentration, $m_s=0.2$ and $m_s=0.4$, $\tau^+=192$, glass.

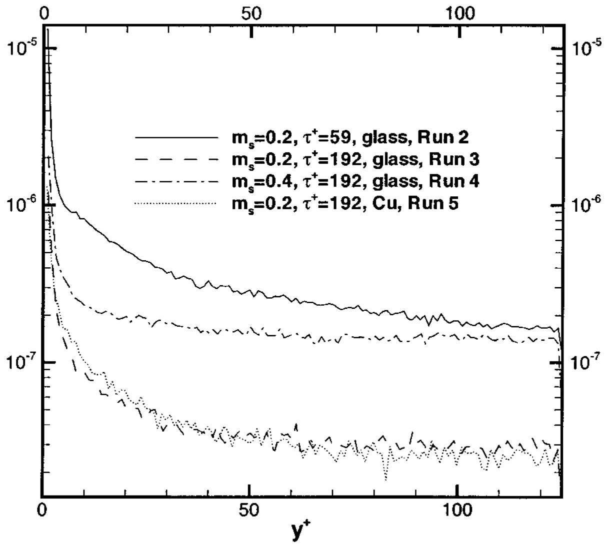

FIG. 12. Dimensionless collision rates.

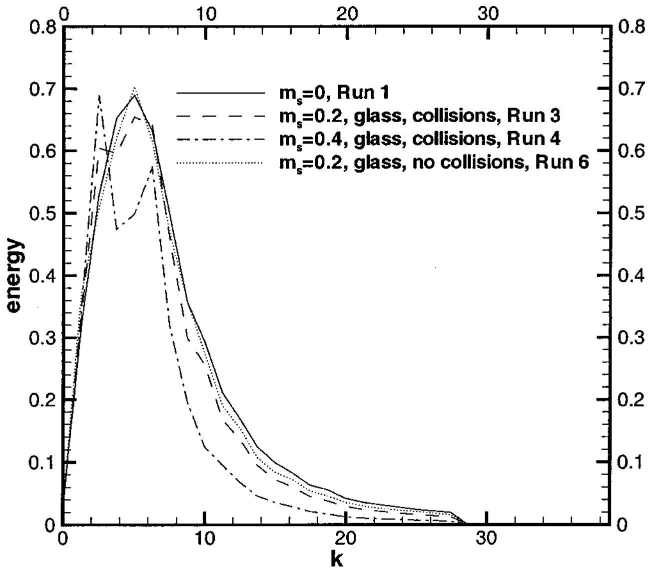

FIG. 13. Two-dimensional energy spectrum at $y^+=32$.

and the weight of the particles. For the simulations in this paper, $1/\mathrm{Fr}=0.31$. Thus, for example, if $m_s=2$, the magnitude of the slope of the mean velocity profile at the walls should be 1.31. The values of this quantity for each run are given in Table III. The deviations from the theoretical values, $\tau^+_{w,\mathrm{th}}$ are likely due to statistical variations in the spatially averaged wall shear stress as a function of time.

The effect on the velocity fluctuation intensities in Fig. 3 is qualitatively similar to the effect of polymeric drag reducing additives (see, for example, Berman[18] and Sureshkumar *et al.*[19]). However, the underlying mechanism may have some differences. For example, polymeric drag reduction is associated with an increase in the spanwise streak spacing. Based on the spanwise correlation of the streamwise component of the wall shear stress, Fortuna and Hanratty[20] found that the spanwise streak spacing was 190 when the drag reduction was 27%. For the present study, when $m_s=0.4$, the increase in volumetric gas flow rate was 13% and this was partly due to the drag of the particles as they sediment. Based on an analogy with polymeric drag reduction, one might expect the streak spacing to be roughly 145 for the above run. Figure 8 indicates the spanwise correlation function of the streamwise component of velocity is relatively little affected by the presence of particles.

Figure 5 shows that, for a given density ratio, the particles with the smaller value of τ^+ have a stronger effect on the gas-phase turbulent intensities. A possible explanation for this phenomenon is that the particles with $\tau^+=59$ respond more to the coherent eddies and, hence, have a stronger feedback effect on the gas-phase turbulence. Particle–particle collisions may also play a role in producing the phenomenon. Figure 12 shows the local collision rates as a function of $y+$. It may be seen that the collision rate for the glass particles with $\tau^+=59$ is an order of magnitude larger than the collision rate for the glass particles with $\tau^+=192$ at the same mass loading. Based on the collision rate and the particle concentration, the time between collisions for a glass particle with $\tau^+=59$ is $O(100)$ wall units. One might expect particle–particle collisions to randomize the particle velocities and to increase the slip velocity between the particles and surrounding gas. Thus, it is plausible that particle–particle collisions would tend to increase the interaction between the particles and the gas.

Some support for the idea that particle–particle collisions may play a role in suppressing gas phase turbulence fluctuations may be found by considering the energy spectrum of the gas-phase turbulence and the gas-phase Reynolds stress. Figure 13 shows the two-dimensional energy spectrum at $y^+=32$ for the particle-free case and three runs in which glass particles were present. In all cases, it may be seen that the particles tend to suppress the small wavelengths. It may also be seen that increasing the mass loading from 0.2 to 0.4 increases the suppression of small wavelengths. There is also a tendency for energy to accumulate in large wavelengths as the mass loading is increased. In Run 6, particle collisions were "turned off." Otherwise, Run 6 is identical to Run 3. It may be seen that, when particle–particle collisions do not occur, the suppression of small wavelengths is reduced. One may also observe that there is less distortion of the energy spectrum for large wavelengths.

Figure 14 shows the gas-phase Reynolds stress for several different cases. It may be seen that the addition of particles reduces the gas-phase Reynolds stress. Also, when the results for Runs 3 and 6 are compared, it may be seen that, when particle–particle collisions are eliminated, the particles have less effect on the Reynolds stress.

To gain insight into the effects of particle feedback on the gas-phase turbulent fluctuations, it is helpful to compute the terms in the energy balances for the fluctuations in the three components of the velocty. In a fully developed turbulent channel flow, the velocity and pressure can be decomposed into mean and fluctuating parts, $(U+u,v,w)$ and $P+p'$. The time-averaged value of each term in the energy balance equation is a function only of *y*. After averaging the kinetic-energy balance equation over *x*, *z*, and *t*, one obtains the mean and component kinetic-energy balance equations in

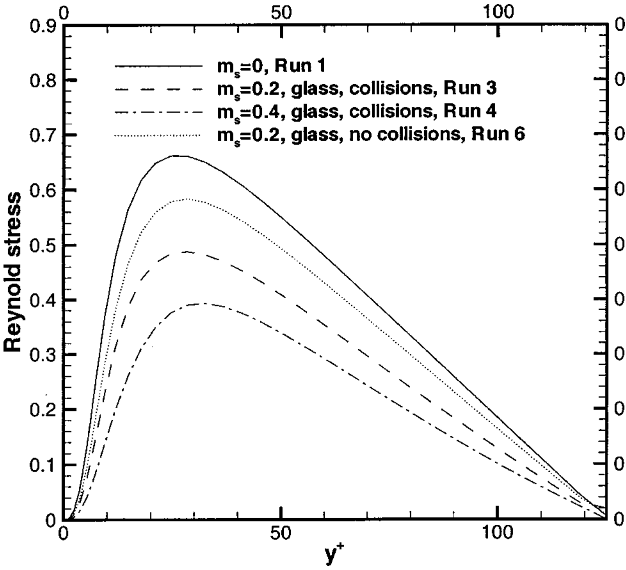

FIG. 14. Gas-phase Reynolds stress.

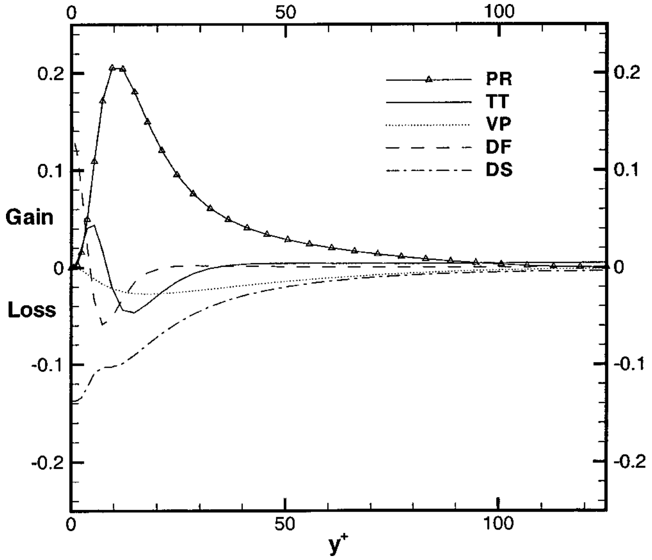

FIG. 15. Energy balance for the *x*-component of velocity, particle-free.

dimensionless form (the overbar here indicates time and *xz*-plane averaging)

$$0=\overline{uv}\frac{dU}{dy}-\frac{d}{dy}(\overline{uv}U)-U\frac{dP}{dx}+\frac{d^2}{dy^2}\left(\frac{1}{2}U^2\right)-\left(\frac{dU}{dy}\right)^2+U\overline{f_x^r}, \tag{11}$$

$$0=-\overline{uv}\frac{dU}{dy}-\frac{\partial}{\partial y}\left(\frac{1}{2}\overline{u^2v}\right)-u\overline{\frac{\partial p'}{\partial x}}+\frac{\partial^2}{\partial y^2}\left(\frac{1}{2}\overline{u^2}\right)-\overline{\left(\frac{\partial u}{\partial x_j}\right)\left(\frac{\partial u}{\partial x_j}\right)}+\overline{uf_x^r}, \tag{12}$$

$$0=-\frac{\partial}{\partial y}\left(\frac{1}{2}\overline{v^3}\right)-v\overline{\frac{\partial p'}{\partial y}}+\frac{\partial^2}{\partial y^2}\left(\frac{1}{2}\overline{v^2}\right)-\overline{\left(\frac{\partial v}{\partial x_j}\right)\left(\frac{\partial v}{\partial x_j}\right)}+\overline{vf_y^r}, \tag{13}$$

$$0=-\frac{\partial}{\partial y}\left(\frac{1}{2}\overline{w^2v}\right)-w\overline{\frac{\partial p'}{\partial z}}+\frac{\partial^2}{\partial y^2}\left(\frac{1}{2}\overline{w^2}\right)-\overline{\left(\frac{\partial w}{\partial x_j}\right)\left(\frac{\partial w}{\partial x_j}\right)}+\overline{wf_z^r}. \tag{14}$$

LO/PR TT VP DF DS FB

The first term (indicated by LO) in Eq. (11) is a loss term. It is the negative of the first term (PR), which is a production term, in Eq. (12). The LO term represents the energy transferred from the mean energy to turbulence component energy. The second term (TT) in Eq. (11) gives the transport rate of the mean flow energy by turbulence. The third term (VP) in Eq. (11) is the work done by the mean pressure gradient interacting with the mean flow; it is usually called the velocity-pressure gradient term. The fourth term (DF) in Eq. (11) gives the viscous diffusion rate of the mean kinetic energy. The fifth term (DS) in Eq. (11) is the viscous dissipation of the mean kinetic energy. The sixth term (FB) in Eq. (11) in the term induced by the particle feedback effects. This term represents the energy transferred from the continuous phase to the particulate phase. Similarly in Eqs. (12)–(14), the second term (TT), third term (VP), fourth term (DF), fifth term (DS), and sixth term (FB) are the turbulence transport term, velocity-pressure gradient term, viscous diffusion term, viscous dissipation term, and feedback induced term, respectively.

Figures 15 and 16 show the terms in the gas-phase energy balance for the *x*-component of velocity. Figure 15 shows the results for the particle-free case ($m_s=0$) and Fig. 16 shows the results for $m_s=0.4$. It may be seen that all terms of the energy balance are reduced by the presence of particles. However, as may be seen Fig. 3, the intensity of the *x*-component of velocity is affected relatively little by the presence of the particles for $m_s=0.4$. Thus, the reduction in

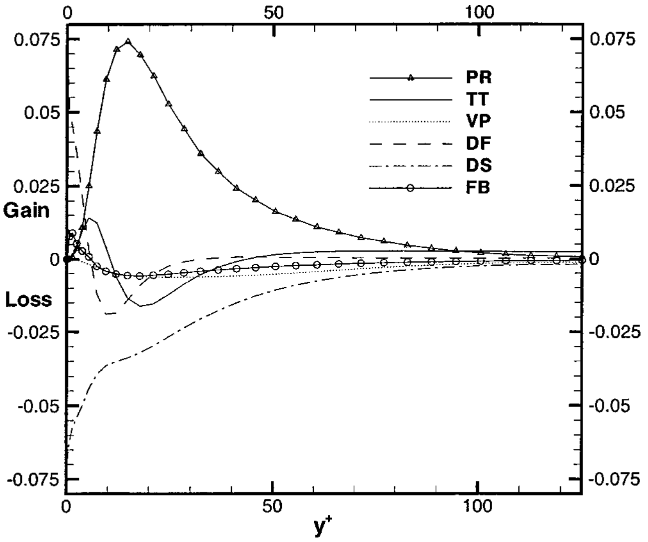

FIG. 16. Energy balance for the *x*-component of velocity, $m_s=0.4$.

TABLE IV. Integral of terms in energy balances, particle-free case.

	PR	TT	VP	DF	DS	Sum
mean flow	−10.5	0	27.5	−0.151	−17.1	−0.325
x	10.5	0	−2.83	−0.0207	−7.70	−0.0249
y	⋯	0	0.991	-1.37×10^{-5}	−0.925	0.0658
z	⋯	0	1.83	-6.29×10^{-3}	−1.94	−0.116

the production of turbulent energy is compensated by the reductions in the dissipation and the velocity-pressure gradient term. This is consistent with the results in Tables IV and V. These tables present the integrals of the terms in the energy balances for the above cases. If one considers the integrals for the *x*-component of velocity, it may be seen that there are reductions of 54% and 55% for the production and dissipation terms while the velocity-pressure gradient term is reduced by 69%. The reduction of the latter term tends to "bottle up" energy in the *x*-component of velocity with the result that the other two components of velocity are significantly suppressed by the presence of the particles. Figure 17 shows the velocity-pressure gradient terms for $m_s=0$ and $m_s=0.4$. It may be seen that the velocity-pressure gradient terms are strongly suppressed by the presence of particles. All terms are reduced by approximately the same factor when particles are present. This is consistent with the fact that the intensities of the normal and spanwise components of velocity are reduced by approximately the same factor since the transfer of energy from the streamwise component of velocity to the other components is reduced.

Another striking feature of the results in Figs. 15 and 16 is that the feedback term is relatively small in comparison with the largest terms. Thus, the particles have an indirect effect on the flow of energy from the mean flow to the turbulent fluctuations.

As the particle loading increases, the particles carry an increasing fraction of the energy and momentum of the two phase flow and the energy balance for the gas phase becomes less significant to the overall budget

B. Particle concentration distribution

In the low concentration limit, several numerical studies[15,21,22] indicated that particles with a broad range of values of τ^+ tend to accumulate near the walls of a vertical channel. Particle inertia is responsible for this phenomenon. Particles tend to travel closer to the walls than the fluid elements that bring them into or near the viscous sublayer. Some particles strike the wall and, in the present study, rebound. However, other particles lack sufficient momentum to reach the closest wall and are "trapped" in the viscous wall region for large periods of time. Figure 11 shows that the accumulation of particles near the walls is diminished when the mass loading increases. This decrease is caused by particle collisions. As mentioned earlier, to demonstrate the importance of particle–particle collisions, in Run 6, particle collisions were turned off. In Fig. 18, the concentration profiles of the two runs are compared. It may be seen that, when particle–particle collisions are eliminated, the particles exhibit a much greater tendency to accumulate near the walls. This may be because collisions tend to decorrelate particles with the coherent eddies that are responsible for the accumulation. Figure 12 shows the dimensionless local collision rate as a function of y^+. If one computes the number of collisions per unit time in the viscous sublayer, one finds that, in a time of $O(100)$ wall units, the number of collisions is on the order

TABLE V. Integral of terms in energy balances, $m_s=0.4$.

	PR	TT	VP	DF	DS	FB	Sum
mean flow	−4.82	0	29.7	−0.138	−16.6	−5.46	2.70
x	4.82	0	−0.890	0.0105	−3.44	−0.511	−0.0251
y	⋯	0	0.389	-3.34×10^{-6}	−0.262	−0.0544	−0.0723
z	⋯	0	0.597	-1.18×10^{-3}	−0.542	−0.0898	−0.0363

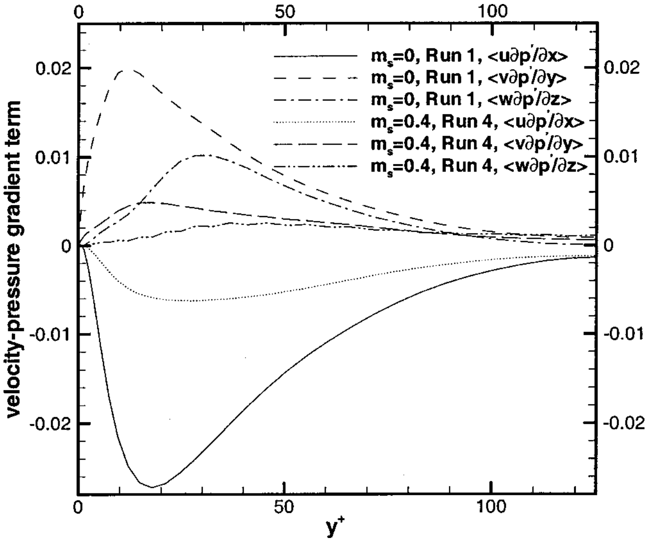

FIG. 17. Velocity-pressure gradient terms (in wall units) in the component energy balances for $m_s=0$ and 0.4, $\tau^+=192$, glass.

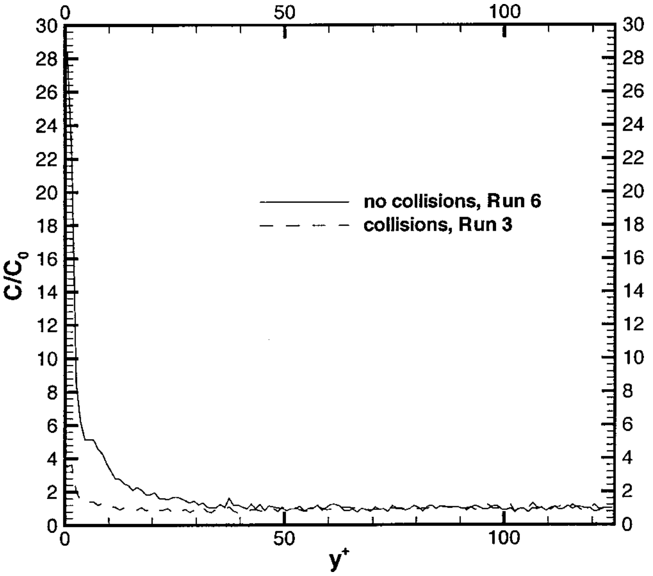

FIG. 18. Normalized particle concentration, $m_s=0.2$, $\tau^+=192$, glass, no collisions.

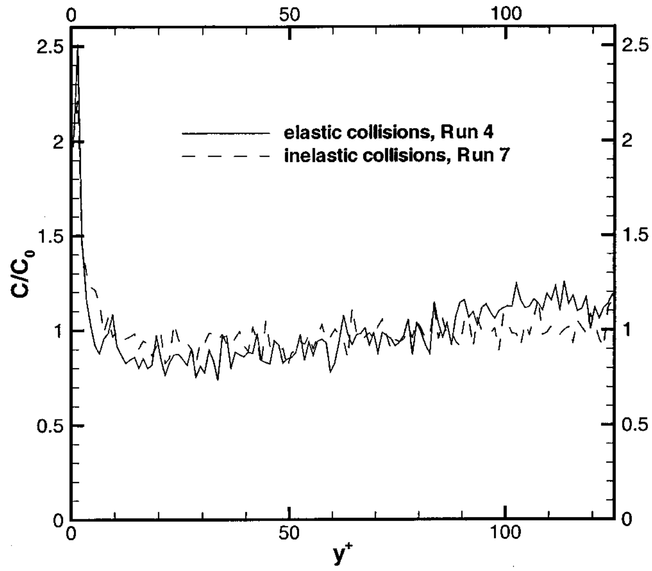

FIG. 19. Normalized particle concentration, $m_s=0.4$, $\tau^+=192$, glass, inelastic collisions, and elastic collisions.

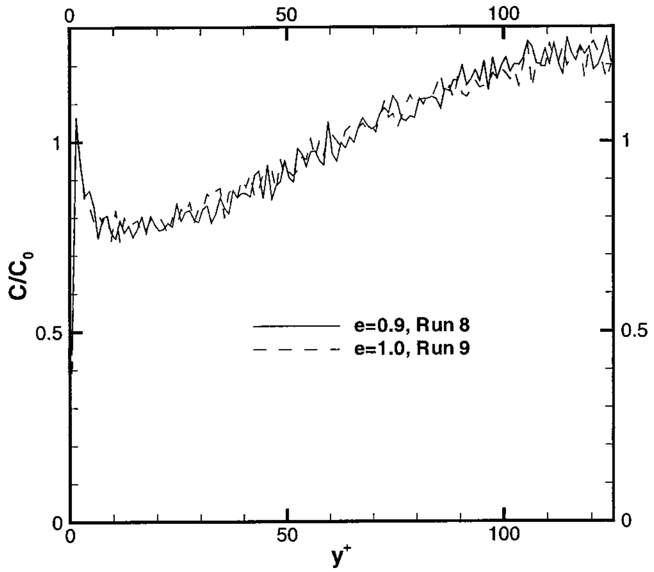

FIG. 20. Normalized particle concentration, $m_s=2.0$, $\tau^+=192$, glass, inelastic collisions, and elastic collisions.

of the number of particles in the sublayer. Without collisions, particles can have much larger residence times in the sublayer because of the small turbulence level in the sublayer.

In this study, the mechanism that leads to accumulations of particles near the channel walls is different from the "turbophoresis" phenomenon identified by Caporaloni *et al.*[23] and, independently, by Reeks.[24] Turbophoresis results from small random steps taken by a particle in response to the surrounding fluid turbulence. If there is a gradient in the intensity of the turbulence, the particles will tend to migrate to regions of lower turbulence intensity since they have a longer residence time in those regions. The particle in this study have large values of τ^+ which causes them to move along roughly straight lines over relatively large distances.

Inelastic particle–particle collisions can also cause particles to accumulate near the walls (see, for example, Hrenya and Sinclair[25]). However, for the concentration range considered in the present study, virtually the same results were obtained when the coefficient of restitution was chosen to be 0.9 instead of 1 as may be seen in Figs. 19 and 20.

As may be seen in Fig. 20, the particle concentration exhibits a maximum in the middle of the channel for $m_s=2$. The cause of this maximum is not clear. Although Fig. 21 shows that the intensity of the normal component of the particle velocity has a minimum at the channel middle, the minimum does not seem deep enough to explain the accumulation of particles. It seems more likely that the accumulation is related to the suppression of the gas-phase turbulent fluctuations seen in Fig. 4. The high-collision frequency may also play a role. For $m_s=2$, the mean time between collisions is roughly 25 wall units. Thus, the distance between collisions is small compared to the channel width.

Another interesting feature of Fig. 21 is that the two transverse components of particle velocity are larger for $m_s=2$ than for $m_s=0.2$ even though the x-component of particle velocity is smaller. Thus, there is a tendency towards isotropy (although the particle velocities are still very anisotropic for $m_s=2$). This is consistent with the increased importance of particle–particle collisions.

VII. CONCLUSIONS

This paper has presented results for the behavior of particle-laden flows in vertical channel flows. For small mass loadings, the particles produce an increase in the mean gas velocity, while, for the largest mass loading, the reverse was true. For small mass loadings, there is a decrease in the fluctuation intensities of the normal and spanwise components of velocity. The particles have a large effect on the velocity-pressure gradient terms in the turbulence energy balances that inhibits the transfer of energy from the streamswise component of velocity to the other two components of velocity. This results in greater anisotropy in the turbulence.

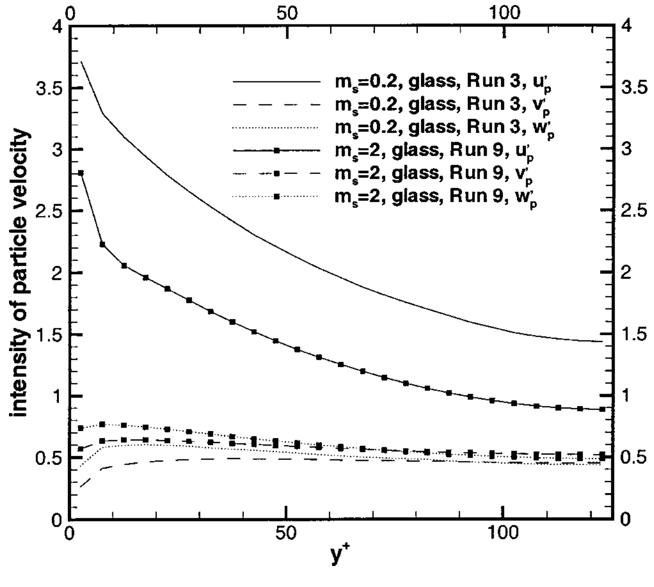

FIG. 21. Particle turbulent intensities (in wall units), $m_s=0.2$ and $m_s=2$.

Although there was no significant increase in the spanwise streak spacing, the streamwise two point correlation of the streamwise component of velocity indicated a suppression of small scale fluctuations. This may also be seen in contour plots of the fluctuating part of the streamwise component of velocity.

Particle–particle collisions significantly reduce the tendency of particles to accumulate near the walls of the channel. It makes little difference whether the collisions are elastic or inelastic. Particle–particle collisions also seem to play a significant role in suppressing the gas-phase turbulence.

For the largest mass loading considered, the gas-phase turbulence is strongly suppressed by the particles. Also, the particle concentration exhibits a maximum in the middle of channel that appears to be caused, in part, by turbophoresis.

ACKNOWLEDGMENTS

This work was supported by DuPont Central Research & Development. The programs and many techniques were developed with support from the Engineering Research Program of the Office of Basic Energy Sciences at the Department of Energy under Contract No. DE-FG02-88ER13919. We acknowledge the support and facilities of the National Center for Supercomputing Applications at the University of Illinois at Urbana, Illinois.

[1] G. Hetsroni, ''Particle-turbulence interaction,'' Int. J. Multiphase Flow **15**, 735 (1989).

[2] R. A. Gore and C. T. Crowe, ''Modulation of turbulence by a dispersed phase,'' J. Fluids Eng. **113**, 304 (1991).

[3] K. Squires and J. K. Eaton, ''Particle response and turbulence modification in isotropic turbulence,'' Phys. Fluids A **2**, 1191 (1990).

[4] S. E. Elghobashi and G. C. Truesdell, ''On the two-way interaction between homogeneous turbulence and dispersed solid particles,'' Phys. Fluids A **5**, 1790 (1993).

[5] C. T. Crowe, M. P. Sharma, and D. E. Stock, ''The particle-source in cell method for gas droplet flow,'' ASME J. Fluids Eng. **99**, 325 (1977).

[6] Y. Pan and S. Banerjee, ''Numerical simulation of particle interactions with wall turbulence,'' Phys. Fluids **8**, 2733 (1996).

[7] M. R. Maxey and B. K. Patel, ''Forced-coupled simulations of particle suspensions at zero and finite Reynolds numbers,'' ASME Fluids Engineering Division Summer Meeting FEDSM'97, June 1997.

[8] M. R. Maxey, B. K. Patel, E. J. Chang, and L.-P. Wang, ''Simulations of dispersed turbulent multiphase flow,'' Fluid Dyn. Res. **20**, 143 (1997).

[9] J. D. Kulick, J. R. Fessler, and J. K. Eaton, ''Particle response and modification in fully turbulent channel flow,'' J. Fluid Mech. **277**, 109 (1994).

[10] M. Chen, K. Kontomaris, and J. B. McLaughlin, ''Direct numerical simulation of droplet collisions in a turbulent channel flow. Part I: collision algorithm,'' Int. J. Multiphase Flow **24**, 1079 (1998).

[11] M. Chen, K. Kontomaris, and J. B. McLaughlin, ''Direct numerical simulation of droplet collisions in a turbulent channel flow. Part II: collision rates,'' Int. J. Multiphase Flow **24**, 1105 (1998).

[12] Y. Yamamoto, T. Tanaka, and Y. Tsuji, ''LES of gas-particle turbulent channel flow (the effect of inter-particle collision on structure of particle distribution),'' Third International Conference on Multiphase Flow, ICMF'98, Lyon, France (1998).

[13] M. Sommerfeld, ''Numerical calculation of particulate flows in process equipment,'' *ECCOMAS 98* (Wiley, New York, 1998).

[14] M. Chen and J. B. McLaughlin, ''A new correlation for the aerosol deposition rate in vertical ducts,'' J. Colloid Interface Sci. **169**, 437 (1995).

[15] J. B. McLaughlin, ''Aerosol particle deposition in numerically simulated channel flow,'' Phys. Fluids A **1**, 1211 (1989).

[16] S. L. Lyons, T. J. Hanratty, and J. B. McLaughlin, ''Large-scale computer simulation of fully developed turbulent channel flow with heat transfer,'' Int. J. Numer. Methods Fluids **13**, 999 (1991).

[17] R. W. Hockney and J. W. Eastwood, *Computer Simulation Using Particles* (Institute of Physics, Bristol, 1988).

[18] N. S. Berman, ''Drag reduction by polymers,'' Annu. Rev. Fluid Mech. **10**, 47 (1978).

[19] R. Sureshkumar, A. N. Beris, and R. A. Handler, ''Direct numerical simulation of the turbulent channel flow of a polymer solution,'' Phys. Fluids **9**, 743 (1997).

[20] G. Fortuna and T. J. Hanratty, ''The influence of drag-reducing polymers on turbulence in the viscous sublayer,'' J. Fluid Mech. **53**, 575 (1972).

[21] G. A. Kallio and M. W. Reeks, ''A numerical simulation of particle deposition in turbulent boundary layers,'' Int. J. Multiphase Flow **15**, 433 (1989).

[22] J. W. Brooke, K. Kontomaris, T. J. Hanratty, and J. B. McLaughlin, ''Turbulent deposition and trapping of aerosols at a wall,'' Phys. Fluids A **4**, 825 (1992).

[23] M. Caporaloni, F. Tampieri, F. Trombetti, and O. Vittori, ''Transfer of particles in nonisotropic air turbulence,'' J. Atmos. Sci. **32**, 565 (1975).

[24] M. W. Reeks, ''The transport of discrete particles in inhomogeneous turbulence,'' J. Aerosol Sci. **14**, 729 (1983).

[25] C. M. Hrenya and J. L. Sinclair, ''Effects of particle-phase turbulence in gas-solid flows,'' AIChE J. **43**, 853 (1997).